Complex eikonal methods applied to geodesic acoustic mode dynamics

F. Palermo,[1, a)] E. Poli,[1] and A. Bottino[1]
Max-Planck-Institut für Plasmaphysik, Garching, Germany.

(Dated: 5 February 2020)

Techniques developed in the domain of optical theory are applied to investigate the behavior of Geodesic Acoustic Modes (GAMs). In this context, we show that this approach represents a powerful basis for the description of many characteristics of radial propagation and spreading of GAMs. The most attractive feature of these techniques is represented by their universality and intuitive applicability. We present and apply two different complex-eikonal methods able to describe the spreading of GAMs in terms of local plane waves. The methods are the "inhomogeneous wave tracking" and the "paraxial WKB" theory respectively. We demonstrate their applicability and efficacy to the GAM dynamics problem by means of a comparison with gyrokinetic simulations.

Keywords: Geodesic Acoustic Mode, complex-eikonal theory, paraxial WKB theory, dispersion

I. INTRODUCTION

The achievement of nuclear fusion is strongly related to the understanding of the non-linear mechanisms by which the turbulence self-organizes in convective structures such as streamers and zonal flows[1–9]. The latter are modulated by, and interact with, a multitude of other structures, instabilities, waves and so on, regulating the energy transport properties in tokamak devices. The zonal flow presents an oscillatory counterpart named geodesic acoustic mode (GAM) that is specific of the toroidal tokamak geometry[10]. This oscillation corresponds to an electrostatic potential perturbation with a poloidal $m = 0$, toroidal $n = 0$ wave number coupled via tokamak curvature to the pressure $m = 1$, $n = 0$ mode; from which the appellation of "geodesics". The studies of GAMs are the most flourishing area in zonal flow experiments. Geodesic acoustic modes (GAMs) are non linearly driven and play an important role in establishing the saturated level of turbulence in tokamaks[11]. GAM structures have been also investigated in neoclassical transport context for tokamak and helical systems[12,13]. Many devices have provided information on the basic features of GAMs, such as the axisymmetric structure, the dispersion relation, the couplings with turbulence and the accompanying density fluctuations[14–16]. So far, most of the observations show good agreement with the present predictions of theory. For example, it has been observed, the essential dependence of the GAM frequency obeys to the theoretical expectation[17–19].

However, the experiments of zonal flows and GAMs are still developing with abundant potentialities, seeing as how a number of issues remain to be explored. For example, GAMs interact with turbulence in an environment in which the plasma shape and profile gradients strongly affect its local and global properties. Temperature and density gradients influence the amplitude of GAMs by regulating both drive and damping in a not completely understood manner. The temperature profile, in particular, regulates the plasma instabilities in tokamaks via e.g. the ion temperature gradient (ITG) modes, trapped electron modes (TEM), electron temperature gradient (ETG) modes and at the same time can strongly influence the damping of GAMs. In fact, the local dependence of the GAM frequency on the plasma parameters generates a continuum spectrum in tokamak plasmas. This continuum is at the basis of the formation of fine structures on GAM via the Phase-mixing process (see Ref. 17). This latter is a conservative process that *per se* is not able to generate a damping. However, in the presence of a temperature gradient, the damping of GAMs can be strongly amplified by means of the combined action of Phase-mixing and Landau damping via the Phase-mixing/Landau (PL) mechanism (see Ref. 20 and Ref.s 21–23). A remarkable aspect about GAMs is that the continuum spectrum not always is present in the experiments and GAM mode can occur at a constant frequency along the radius. In fact, at a particular radial location, it is often possible to identify GAMs at two distinct frequencies, or to observe separate radial intervals over which the GAM occurs at different but constant frequencies within each interval (eigenmodes)[14]. Thus, GAM often can be approximated with a Gaussian packet. In more recent works, GAM has been shown to form radial Airy function-like eigenmodes when finite Larmor radius effects are included[24]. In DIIID it appears that both continuum and eigenmode GAM structures can be realized experimentally[25]. Moreover, temperature gradient is correlated with the radial propagation of GAMs but also in this case, details of phenomena need to be clarified. The question of the GAM propagation in the radial direction has been investigated in multiple experiments. The results of these experiments do not give one single answer, as GAM propagation has been observed in both radially inward and outward directions with different velocities[26–29]. In some case a spreading of GAM has been observed with the separation of the primary GAM structure in two parts that successively move in opposite directions[30]. The question about the direction of propagation of GAM has been discussed in Ref. 23

[a)] Electronic mail: francesco.palermo@ipp.mpg.de

and 31. Moreover, the velocities of GAM observed in the experiment are larger than that predicted by the linear theory[33]. Recently, it has been shown that GAMs can accelerate increasing their velocity and reducing the discrepancy between linear theory and experiments[23]. In this puzzling picture, the interaction between GAM and turbulence strongly increases the complexity of the problem[17].

In this context, an aspect that has been neglected in literature, but that could be important in the interaction between turbulence and GAM, is represented by the spreading of the GAM packet due to dispersion relation. Although, for typical tokamak values of parameters this effect appears lower than one of dissipation it could play an important role in the experiments- for example - in the case in which the drive is compensated by the dissipation. In front of the complexity of these problems, the investigation of GAM dynamics, zonal flows and other structures certainly requires new simulations and new experiments. However, in parallel to these studies, it is crucial to develop and to apply new techniques and diagnostics able to capture and to distinguish the essential characteristics of specific mechanisms. For this purpose, in this work we apply techniques derived from the field of optics to the GAM oscillations. In this context, we show that these theories represent a useful instrument for the description of many characteristics of radial propagation and spreading of GAMs. The most attractive feature of these methods is represented by their universality and intuitive applicability. Moreover, in many cases optical techniques are the only possible approximation for calculating wave fields in the presence of homogeneous and inhomogeneous media. Ray tracing technique of geometrical optics is the most powerful and widespread method of solving wave equation in the short-wavelength limit. It is used in numerous applications of optics, seismology, physics of fluids and solids, quantum mechanics, plasma physics and many other fields. This method makes use of an asymptotic expansion of the sought solution and reduces the wave equation to an infinite set of coupled equations for successive terms of the expansion. The zero-order term is know as the eikonal equation.

Although refraction is correctly accounted in this method, typical wave behaviors, like interference and diffraction, which could be regarded as an interaction between different rays, cannot be described by the ray tracing technique. These effects can, however, become significant, if one is concerned, for instance, with highly collimated or focused microwave beams, which are of great importance for the physics of fusion devices. They are employed for diagnostic purposes, to improve spatial resolution, as well as, in resonant heating and current drive experiments, to increase the localization of the absorbed power. Diffraction effects, not described by the usual geometric optics, can be included adding a complex phase allowing to describe in this way several interesting new characteristics of different phenomena. By using a complex-eikonal description, in the following, we present and apply two different optical methods able to describe the spreading of GAMs in terms of local inhomogeneous plane waves. The adopted methods are the "inhomogeneous wave tracking"[34–36] and the "paraxial WKB (pWKB) approximation"[38–40]. Both of them present several advantages. The former is based on a set of partial differential equations and in several cases gives a direct intuitive picture of the physical dynamics of the phenomena. The latter method is based on a Hamiltonian description and deals with a set of ordinary differential equations that present an important advantage from a computational point of view. These methods have been previously applied to the problem of heating, current drive and plasma diagnostics with microwave beams in fusion devices. Due to the different advantages related to the mentioned methods, in the following we present both of them and apply them to GAM dynamics and we demonstrate their validity and efficacy by means of a comparison with gyrokinetic simulations.

The rationale of the work are introduced in Section 2. The optical methods and the analytical results are described in Section 3 and Section 4. The simulation results and the comparison with the theory are shown in Section 5. The conclusions of the work are given in Section 6.

II. NUMERICAL MODEL AND PHYSICAL APPROACH

A. Numerical gyrokinetic code ORB5

In this section we briefly describe the equations used in the code ORB5[41,42,44]. This code uses a Monte Carlo Lagrangian Particle-in-Cell method for solving the Vlasov equation[43]. The model solved in the code is constructed from a gyrokinetic Lagrangian and it is described in detail in reference[45].
The gyrokinetic Lagrangian corresponding to the electromagnetic ORB5 model is

$$L = \sum_{sp} \int dW\, dV \Big(\big(e\mathbf{A} + p_{\|}\mathbf{b}\big) \cdot \dot{\boldsymbol{R}} + \frac{m_{sp}c}{q_{sp}} \mu\dot{\alpha} - H \Big) f_{sp} + \int \frac{|\nabla_{\perp} A_{\|}|^2}{8\pi} dV \quad ,$$

$$H = \frac{p_{||}^2}{2m_{sp}} + \mu B + q_{sp} J_0 \left(\Phi - \frac{p_{||}}{m_{sp}c} A_{||} \right) + \frac{q_{sp}^2}{2m_{sp}c^2} (J_0 A_{||})^2 - \frac{m_{sp}c^2}{2B^2} |\nabla_{\perp}\phi|^2 \quad ,$$

in which the coordinates are the gyrocenter position $\boldsymbol{R}$, the adiabatic invariant μ, the gyro angle α and the canonical parallel momentum $p_{\|} = m_{sp}U + (q_{sp}/c)J_0 A_{\|}$, where U is the parallel velocity; dV and dW are the volume elements in physical and velocity space respectively. In the last expression $\boldsymbol{B}$ is the equilibrium magnetic field and ϕ is the perturbed electrostatic potential operator. $A_{\|}$

is the parallel component of the perturbed vector potential, J_0 is the gyro-average operator, q_{sp} and m_{sp} are the charge and the mass of particle species sp respectively and c is the speed of light. The particle gyrocenter trajectories are derived from the variational principles on the action and can be written in the following explicit form:

$$\dot{\boldsymbol{R}} = \frac{1}{m_{sp}}\left(p_{\parallel} - \frac{q_{sp}}{c}J_0 A_{\parallel}\right)\frac{\boldsymbol{B}^*}{B^*_{\parallel}} + \frac{c}{q_{sp}B^*_{\parallel}}\boldsymbol{b}\times\left[\mu\nabla B + q_{sp}\nabla J_0\left(\phi - \frac{p_{\parallel}}{m_{sp}c}A_{\parallel}\right)\right] \quad (1)$$

$$\dot{p_{\parallel}} = -\frac{\boldsymbol{B}^*}{B^*_{\parallel}}\cdot\left[\mu\nabla B + e\nabla J_0\left(\phi - \frac{p_{\parallel}}{m_{sp}c}A_{\parallel}\right)\right] \quad (2)$$

where $\boldsymbol{B}^* = \nabla\times\boldsymbol{A}^*$, $\boldsymbol{A}^* \equiv \boldsymbol{A} + (p_{\parallel}/q_{sp})\boldsymbol{b}$ and $\boldsymbol{b} = \boldsymbol{B}/B$. The distribution function is split into a constant in time background, f_0, and a fluctuating part δf. Only the time varying part of the distribution function, δf, is discretized using Monte Carlo markers and it is evolved (in the absence of sources and collisions) according to the gyrokinetic Vlasov equation:

$$\frac{\mathrm{d}\delta f_{sp}}{\mathrm{d}t} = -\frac{\partial f_0}{\partial \boldsymbol{R}}\cdot\dot{\boldsymbol{R}} - \frac{\partial f_0}{\partial p_{\parallel}}\dot{p_{\parallel}} \quad . \quad (3)$$

Energy and momentum conservations can be proved via gyrokinetic field theory[45]. To evolve self-consistently the perturbed electrostatic and magnetic potentials, the Vlasov equation should be coupled with equations for the fields. Those are obtained by taking functional derivatives of the action functional with respect the perturbed potential, leading to a polarization equation for ϕ and the Ampére law for $A_{||}$. In this work we have used the electrostatic limit of the model with a single ion species and adiabatic electrons. The corresponding equations are obtained by setting $A_{\parallel} = 0$ in the previous equations and by assuming a fluid like response of the electrons density to the potential perturbation. The corresponding polarization equation is:

$$\frac{n_0}{T_e}(\phi - \bar{\phi}) - \nabla_{\perp}\frac{m_i n_0 c^2}{q_i B^2}\nabla_{\perp}\Phi = \int dW q_i J_0 \delta f \quad (4)$$

n_0 is the equilibrium density, T_e is the electron temperature and $\bar{\phi}$ is the flux surface average of the electrostatic potential. The full derivation and disctretization of the electrostatic model can be found in Ref. 43. In the code, a set of straight field line coordinates (s, χ, φ) is used, with $s = \sqrt{\psi/\psi_{edge}}$, where ψ is the poloidal magnetic flux, and χ is the magnetic poloidal angle

$$\chi = \frac{1}{q(s)}\int_0^{\theta}\frac{B\cdot\nabla\varphi}{B\cdot\nabla\theta'}d\theta' \quad (5)$$

where θ is the geometric poloidal angle, φ the toroidal angle and $q(s)$ is the safety factor. The polarization equation is solved using finite elements (B-splines). The boundary conditions on the fields are unicity condition (solution does not depend on magnetic angle) at the magnetic axis and $\phi = 0$ at the plasma boundary. Regarding particles, they are reflected with $\chi = -\chi$ when they exit the plasma boundary. In the code, the time t is normalized to the inverse of the ion cyclotron frequency $\Omega_i = q_i B_0/m_i$ (assuming $c = 1$), the radial direction is normalized to $\rho_s = \sqrt{k_B T_{e,0} m_i}/(q_i B_0)$ with $T_{e,0}$ the electron temperature, and the potential is given in $\phi_0 = k_B T_{e,0}/e$ units. The quantity B_0 is calculated at the magnetic axis, while $T_{e,0}$ is calculated in the middle of the radial domain. The ion Larmor radius is defined as $\rho_i = \sqrt{2}\sqrt{T_{i,0}/T_{e,0}}\rho_s$ with $T_{i,0}$ the ion temperature in the middle of the radial domain.

B. Rationale and physical motivations

We present the principal aspects of the optical approach to the problem of the GAM behavior. In particular, we discuss how it is possible to describe the time evolution of GAMs starting from a particular combination of the principal equilibrium parameters. In this way, we are able to associate a "GAM refraction-index" n_G to the GAM structures related to the equilibrium conditions. To this purpose we write the two dimensional Helmholtz equation:

$$(\nabla^2 + k_0^2 n_0^2)E = \left[\frac{\partial}{\partial x^2} + \frac{\partial}{\partial y^2} + n_0^2\right]E = 0 \quad (6)$$

where we include the vacuum wave vector $k_0 = \omega/c$ in the definition of the refraction index n_0 which has here the dimensions of an inverse length. We observe that Eq. 6 is valid under the condition that the variations of the associate index of refraction n_0, in the spatial (x, y)-plane, are not very strong. More specifically, the L_T scale length characterizing the medium inhomogeneity in the different x and y directions must be larger than the typical wavelength λ of the waves that propagate in the medium.

We observe that GAMs are one-dimensional radial structures that oscillate in an equilibrium that in the following we assume to be fixed in time. Thus, their one-dimensional oscillations appear as a wave that propagates in a space-time plane. This wave is characterized by a "wave length" $T_0 = 2\pi/\omega_G$, that in this case is related to the GAM frequency. In other words, the wave vector $k_0^2 n_0^2$ is here replaced by the GAM frequency ω_G^2 that appears in the dispersion relation of GAMs:

$$\omega^2 = \omega_G^2(1 + \alpha_1 k_r^2 \rho_i^2) \quad (7)$$

We recall that Eq. 7 represents the GAM frequency at the second-order of accuracy in $k_r\rho_i$ where the sign and the value of the coefficient α_1 depend on the ratio $\tau_e = T_e/T_i$. For the sake of clarity we report the explicit expression of α_1 used in the work (see Ref. 17, 23, and

50):

$$\alpha_1 = \frac{1}{2}\Big[\frac{3}{4} - \Big(\frac{7}{4}+\tau_e\Big)^{-1}\Big(\frac{13}{4}+3\tau_e+\tau_e^2\Big) + \Big(\frac{7}{4}+\tau_e\Big)^{-2}\Big(\frac{747}{32}+\frac{481}{32}\tau_e+\frac{35}{8}\tau_e^2+\frac{1}{2}\tau_e^3\Big)\Big]$$

We observe that the α_1 parameter becomes negative for $\tau_e \gtrsim 5.45$.

Thus, we can find a strict correspondence between Eq. 6 and the wave equation describing the temporal evolution of GAMs (cf. Eq. 14 of Ref. 33):

$$(\tilde{\nabla}^2+1)E = \Big[+\frac{1}{\omega_G^2}\frac{\partial^2}{\partial t^2} - \alpha_1\rho_i^2\frac{\partial^2}{\partial r^2}+1\Big]E = 0 \qquad (8)$$

We note that Eq. 8 appears as the normalized version of Eq. 6 where $x \to \omega_G t$ and $y \to r/\sqrt{|\alpha_1|}\rho_i$ are the normalized time and radial variables respectively and where the square index of refraction n_G^2, which should appear as the last term within the square brachets in Eq. 8, becomes equal to the unity.

The correspondence between Eq. 6 and Eq. 8 implies that the temporal variation of GAM can be treated as a spatial variation. This means that all the GAM time variations appear frozen in the (x,y)-plane. Therefore, in this paper we consider a GAM wave with an initial "wave-vector" ω_G that propagates along the x (temporal) direction in a (x,y)-medium characterized by an inhomogeneity with a scale length L_T along the y (radial) direction. We observe that the treatment described hereafter include also the case in which the equilibrium evolves in time under the condition that the scale length L_T associated to the temporal variation is larger than $2\pi/\omega_G$.

III. COMPLEX-EIKONAL THEORY I: INHOMOGENEOUS WAVE TRACKING

Starting from the previous considerations, we summarize the essential aspects of the complex eikonal theory developed principally in Ref. 34–36 and we apply it to the prediction of the time evolution of GAMs. Moreover, we extend the theory to the inhomogeneous case in which we consider a constant temperature gradient. As mentioned in the introduction, this theory represents a very useful development of the classical eikonal theory. This latter, it is known, well describes the curved spatial path of ray in weakly inhomogeneous media. Complex eikonal theory can also describes phenomena associated with Gaussian beams such as broadening due to diffraction and interference effects. We emphasize that these effects act also in the presence of a constant refraction index. This method is applied here to describe the time evolution of a one-dimensional Gaussian GAM signal.

In order to introduce this method, we observe that the common ray approach to the solution of the Helmholtz equation in the short wave length limit leads to the lowest order in k_0^{-1} to the eikonal equation, which determines the eikonal function:

$$(\nabla S)^2 = n^2 \qquad (9)$$

The next-order terms represent the transport equations for the amplitude E. For the sake of simplicity and in order to focus attention on the primary idea of the work (applicability of complex optical methods to the GAM temporal evolution), the treatment of GAM dynamics is limited to eikonal term. The evolution of the wave amplitude, including damping effects, will be considered in a future publication.

In order to take into account the effects of spreading, describing in this way not only a plane wave but also a packet signal, we consider a complex phase (eikonal) S:

$$S = s + i\phi \qquad (10)$$

that substituted in Eq. 9 allows us to obtain:

$$(\nabla s)^2 - (\nabla\phi)^2 = n^2 \qquad \nabla s\cdot\nabla\phi = 0 \qquad (11)$$

It is important to emphasize that in the eikonal theory the trajectories on which ϕ is constant (phase paths) are perpendicular to the trajectories on which s is constant (equiphase contours). By observing Eq. 7 we have that the curvature sign of equiphase contour is related to the sign of α_1 that, we recall, depends on τ_e (see Ref.s 17, 23, and 50). Thus, for $\alpha_1 < 0$ the signs of the different terms in Eq. 8 are in agreement with those in Eq. 6. For $\alpha_1 > 0$ the signs are different, but by considering the opposite value of the parameter the second relation of Eq. 11 continue to be valid. We define the unit vector $\boldsymbol{\tau}$ along the direction of ∇s and the unit vector $\boldsymbol{z}$ along the direction of $\nabla\phi$ respectively.

We can write:

$$\Big(\frac{ds}{d\tau}\boldsymbol{\tau}\Big)^2 - \Big(\frac{d\phi}{dz}\boldsymbol{z}\Big)^2 = n^2 \qquad (12)$$

By applying the gradient operator to the previous equation we obtain:

$$2\frac{ds}{d\tau}\boldsymbol{\tau}\cdot\nabla\Big(\frac{ds}{d\tau}\boldsymbol{\tau}\Big) - 2\frac{d\phi}{dz}\boldsymbol{z}\cdot\nabla\Big(\frac{d\phi}{dz}\boldsymbol{z}\Big) = 2n\nabla n \qquad (13)$$

By defining $\beta = |\nabla s|$ and $\xi = |\nabla\phi|$ we rewrite Eq. 13 in the following manner:

$$\beta\frac{d}{d\tau}\Big(\beta\boldsymbol{\tau}\Big) - \xi\frac{d}{dz}\Big(\xi\boldsymbol{z}\Big) = n\nabla n \qquad (14)$$

We observe that the derivatives $d\boldsymbol{\tau}/d\tau = K\boldsymbol{z}$ and $d\boldsymbol{z}/dz = -\Gamma\boldsymbol{\tau}$ of the unit vectors $\boldsymbol{\tau}$ and $\boldsymbol{z}$ respectively introduce two new quantities K and Γ. These parameters are related to the radii $1/K$ and $1/\Gamma$ of tangent circumferences (osculating circles) to the phase paths and equiphase contours respectively.

Thus, we rewrite Eq. 13 in two components:

$$\beta^2 K = n\frac{d}{dz}n + \xi\frac{d}{dz}\xi \qquad \xi^2\Gamma = n\frac{d}{d\tau}n - \beta\frac{d}{d\tau}\beta \qquad (15)$$

These two equations take into account the gradient of the index of refraction n and the gradient of the beam profile ξ. The n gradient must be smaller than the gradient of the beam packet. It is interesting to observe that even in the case in which we have a constant refraction index, the curvatures K and Γ can be different from zero. When ξ is constant we find the classical eikonal solution. The previous equations 15 are very useful in order to describe the radial evolution of an initial beam. In a first step, we adopt the treatment of the spatial beam propagation in homogeneous medium[36] putting in evidence the new interpretation and applicability of the method for time evolution of GAM. Successively, we extend this description to the case of the GAM oscillations in the presence of a nonuniform temperature profile.

A. GAM Gaussian beam in homogeneous medium

We consider a GAM represented by the following initial Gaussian beam signal:

$$E(y) = E_0 e^{-\frac{(y-y_0)^2}{W_0^2}} \tag{16}$$

where W_0 is the width of the packet propagating in the (x, y)-plane, in a medium with a constant "GAM refraction-index" n_G that, in our normalized units, is equal to one. By using Eq. 15 for K we calculate $\xi d\xi/dz$ and ndn/dz. At $x = 0$ the directions of $\boldsymbol{\tau}$and $\boldsymbol{z}$ correspond to those of the Cartesian vectors $\hat{\boldsymbol{i}}$ and $\hat{\boldsymbol{j}}$. Therefore, $d/dz \longrightarrow d/dy$. Consequently, because n is constant along y direction, we conclude that the term ndn/dz is equal to zero. At the initial time $x = 0$ we calculate:

$$\xi_0 = |\nabla\phi| = |\frac{2(y-y_0)}{W_0^2}| = \frac{2|p|}{W_0^2} \qquad \frac{d\xi_0}{dz} = \frac{2}{W_0^2}\frac{p}{|p|} \tag{17}$$

where p is a parameter that indicates the distance of a point from the center of the packet. In this way we would like to find the phase path trajectory $y(x, p)$ along the temporal coordinate x for each initial p points of the packet. Finally we calculate β_0^2:

$$\beta_0^2 = n^2 + \xi_0^2 = n_G^2\Big[1 + \frac{4p^2}{n_G^2 W_0^4}\Big] \tag{18}$$

and by using Eq. 15 for K we obtain:

$$K = \frac{4}{n_G^2 W_0^4} p\Big[1 + \frac{4}{n_G^2 W_0^4}p^2\Big]^{-1} \approx p\Big(\frac{4}{n_G^2 W_0^4}\Big) \tag{19}$$

where in the last step we have considered small values of the p parameter. In the previous expressions, we maintain the "GAM refraction-index" n_G in order to express through it, the dispersive properties of the plasma when physical dimensions are reintroduced (see Eq. 25). We recall that $1/K$ is the radius of the osculating circle tangent to the phase path along which $\boldsymbol{\tau}$ moves (see Fig. 1). Consequently $(1/K)d\theta = d\tau$ and $K = d\theta/d\tau$. In our

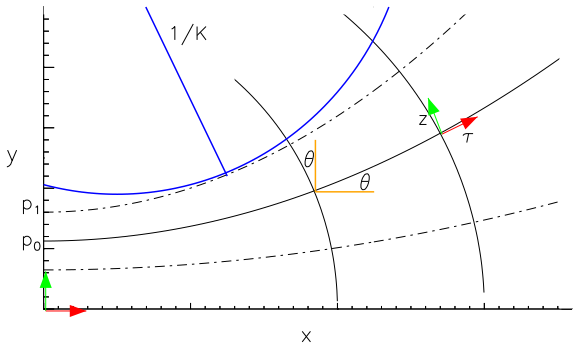

FIG. 1. Trajectories of phase paths along which the vector $\boldsymbol{s}$ moves. Phase paths are characterized by a parameter p. The ϕ quantity is constant along a generic phase path.

geometry, θ is the angle between the x direction and the phase path. Therefore, we have $d\tau\cos\theta = dx$ and we can write:

$$\tan\theta = \frac{dy}{dx} \longrightarrow \frac{d\tan\theta}{dx} = \frac{d\theta}{dx}\frac{1}{\cos^2\theta} = \frac{d^2y}{dx^2} \longrightarrow \frac{d\theta}{d\tau} = \frac{d^2y}{dx^2}\cos^3\theta \tag{20}$$

For small values of θ we have $K = d^2y/dx^2$ and by considering Eq. 19 we write:

$$y(x, p) = \frac{x^2}{2}p\Big(\frac{4}{n_G^2 W_0^4}\Big) + C \tag{21}$$

that describe the time evolution of each radial point p of the Gaussian packet. In order to obtain the value of the constant C we observe that at the time $x = 0$ we have the $y(0, p) = p$ position, hence $C = p$.

We observe that for each p value $\phi = constant$ on a phase path, and $d\phi = \xi dz$ between adjacent paths is also constant. Thus, $\xi(x)/\xi(x_0)$ represents the cross section expansion along the flux tubes.

$$\xi(x_0)dz_0 = \xi(x)dz \longrightarrow \frac{W(x)^2}{W_0^2} = \frac{dz}{dz_0} = \frac{dy\cos\theta}{dp} \approx \frac{dy}{dp} \tag{22}$$

By considering the derivation of Eq. 21, the width $W(x)$ of the Gaussian beam evolves in time with the following expression:

$$W(x)^2 = W_0^2\Big[1 + \frac{4}{n_G^2 W_0^4}\frac{1}{2}x^2\Big] \tag{23}$$

We emphasize that Eq. 21 for phase path trajectories has been obtained by considering the lowest order terms of

the complex eikonal. The wave fronts can be obtained at the same order by considering Eq. 15 for Γ. We observe that there are several ways to explicit the n_G parameter that, we recall, in our normalized variables is equal to one. In order to prepare the comparison between theory and simulations, by considering the previous x, y normalizations and also the normalizations used in the code, we obtain:

$$\frac{W(t)^2}{W_0^2} = \Big[1 + \frac{1}{2}\frac{4(t\Omega_i)^2}{(W_0/a)^4}\frac{\alpha_1^2\rho_i^4}{a^4}\frac{\omega_G^2}{\Omega_i^2}\Big] \tag{24}$$

from which:

$$n_G^2 = \frac{1}{\alpha_1^2\omega_G^2\rho_i^4} \tag{25}$$

In this way we have described what a GAM structure "see" during its oscillations, or in other words, which are the important equilibrium parameters that influence in first approximation the GAM dynamics. We would like to emphasize that a similar description can be applied to other structures in tokamaks such as the drift waves and so on. We note that a treatment of drift-balloning modes in terms of optical pWKB technique has been done in Ref. 37.

B. Inhomogeneous case

Identifying the combination of parameters that can be associated to the like-index of refraction for GAMs allows, as a natural extension of the calculation, the treatment of a nonuniform equilibrium typical of the pedestal region in which these structures evolve. The simple case that we can consider is that of a temperature gradient $1/L_T = -(1/T)dT/dy$ that determines the following ω_G profile:

$$\omega(y) = \omega_G + \frac{d\omega_G}{dy}(y - y_0) = \omega_G\Big[1 - \frac{1}{2}\frac{1}{L_T}(y - y_0)\Big] \tag{26}$$

Consequently also our index of refraction will be influenced by the temperature gradient and by considering the normalization units x, y we have, with $\kappa_T = 1/L_T$:

$$\frac{1}{n(y)} = \frac{1}{n_G}\Big[1 - 0.5\kappa_T(y - y_0)\Big] \tag{27}$$

Then, we calculate the right side of Eq. 15 for K:

$$n\frac{d}{dz}n + \xi\frac{d}{dz}\xi = n_G^2\Big[\frac{0.5\kappa_T}{(1 - 0.5\kappa_T p)^3} + \frac{4p}{n_G^2W_0^4}\Big] \tag{28}$$

Finally we calculate β_0^2:

$$\beta_0^2 = n^2 + \xi_0^2 = n_G^2\Big[\frac{1}{(1 - 0.5\kappa_T p)^2} + \frac{4p^2}{n_G^2W_0^4}\Big] \tag{29}$$

Thus, we can write the inverse of the radius $1/K$ of the osculating circle as:

$$K = \frac{d^2y}{dx^2} = \frac{0.5\kappa_T(1 - 0.5\kappa_T p)^{-3} + 4p/(n_G^2W_0^4)}{(1 - 0.5\kappa_T p)^{-2} + 4p^2/(n_G^2W_0^4)} \approx \tag{30}$$
$$p\Big(\frac{4}{n_G^2W_0^4} + 0.25\kappa_T^2\Big) + 0.5\kappa_T \approx p\frac{4}{n_G^2W_0^4} + 0.5\kappa_T$$

For the phase path trajectory will have thus the following expression:

$$y(x,p) = \frac{x^2}{2}\Big[p\frac{4}{n_G^2W_0^4} + 0.5\kappa_T\Big] + p + y_0 \tag{31}$$

where we have considered approximation for small p and κ_T gradient values in agreement with the optical approximation. The $p = 0$ value in Eq. 31 corresponds to find the trajectory of the center of Gaussian beam that corresponds to the ray-trajectory of the classical eikonal theory:

$$y(x,p) = \frac{\kappa_T}{2}\frac{x^2}{2} \longrightarrow \frac{r(t,p)}{\sqrt{|\alpha_1|}\rho_i} = \frac{1}{2}\sqrt{|\alpha_1|}\rho_i\omega_G^2\frac{\alpha_1}{|\alpha_1|}\frac{1}{L_T}\frac{t^2}{2} \tag{32}$$

where we have added $\alpha_1/|\alpha_1|$ in order to recover the sign of α_1. In this way we obtain the following acceleration:

$$a_c = \frac{1}{2}\alpha_1\rho_i^2\omega_G^2\frac{1}{L_T} \tag{33}$$

Eq. 33 is the same expression obtained in a different way in Ref. 23. It is very interesting to observe how the inverse of the osculating circle radius $1/K$ related to the bend of the spatial trajectory in the eikonal theory assumes here the role of an acceleration.

By rewriting Eq. 31 in the usual coordinates r and t we obtain:

$$r(t,p) = \frac{t^2}{2}\Big[p\frac{4\alpha_1^2\omega_G^2\rho_i^4}{W_0^4} + \frac{1}{2}\alpha_1\rho_i^2\omega_G^2\frac{1}{L_T}\Big] + p + r_0 \tag{34}$$

that includes effects related to the inhomogeneity of the environment and to the shape of the beam via dispersion GAM relation. In particular the term within square brackets is a generalized acceleration associated to a generic p point of the GAM signal.

IV. COMPLEX-EIKONAL THEORY II: PARAXIAL WKB METHOD

As mentioned above, an equivalent description of the dynamics of a packet can be obtained by using a different method based on the paraxial WKB (pWKB) approach. An extensive treatment of the paraxial WKB method can be found in Ref.s 38–40. Here, we introduce the essential aspects of the method and the principal equations useful to investigate GAM dynamics.

As in standard ray tracing, the calculation of the beam evolution according to the pWKB method relies on the

Hamiltonian of geometric optics. In the simple one-dimensional case under consideration, the Hamiltonian takes the very simple form:

$$H = \omega_G^2(1 + \alpha_1 k_r^2 \rho_i^2) - \omega^2 = 0. \tag{35}$$

As in the inhomogeneous wave tracking discussed above, the phase is supposed to be complex, with the imaginary part describing the beam envelop. The properties of the medium are supposed not to vary significantly across the beam, so that the phase can be expanded around a reference curve representing the center of the packet. This curve corresponds to the ray-trajectory obtained with the classical eikonal approach. In one dimension, the (paraxial) expansion reads

$$S(\tau) = S_0(\tau) + k_0(\tau)[r - r_0(\tau)] + \frac{1}{2}s(\tau)[r - r_0(\tau)]^2 + \frac{i}{2}\phi(\tau)[r - r_0(\tau)]^2 \tag{36}$$

When this *ansatz* is substituted in the relevant wave equation (in our case Eq. 8) it leads to the standard ray tracing equation for the center of the packet :

$$\frac{dr_0}{d\tau} = \frac{\partial H}{\partial k_r} \qquad \frac{dk_0}{d\tau} = -\frac{\partial H}{\partial r} \tag{37}$$

The evolution of the beam envelop is calculated along this trajectory as the solution of a complex Riccati equation for the quantity $\overline{s}(\tau) = s(\tau) + i\phi(\tau)$:

$$\frac{d\overline{s}}{d\tau} = -\frac{\partial^2 H}{\partial r^2} - 2\frac{\partial^2 H}{\partial r \partial k_r}\overline{s} - \frac{\partial^2 H}{\partial k_r^2}\overline{s}^2 \tag{38}$$

Also here, we neglect the evolution of the amplitude of the wave packet. In any case, the strength and elegance of the pWKB approach results from the simplification of the problem to a set of ordinary differential equations, for which we are going to discuss some analytic solutions in the remaining part of this section.

A. GAM beam in homogeneous medium

We apply the pWKB method to the GAM problem and we find a direct correspondence with the results discussed in Section III. In the homogeneous case the equation for the evolution of the (complex) beam envelope $\overline{s}$ in the frame of the paraxial WKB method can be written in the form:

$$\frac{d\overline{s}}{d\tau} = -\frac{\partial^2 H}{\partial k_r^2}\overline{s}^2 \tag{39}$$

According to paraxial theory, the coefficient $\partial^2 H/\partial k_r^2$ has to be evaluated at the center of the wave packet. Moreover, in the homogeneous case the position of the center of the packet and the wave vector do not evolve in time and for a symmetric initial spectrum it is $k_r = 0$. Therefore, we can write:

$$\frac{d\overline{s}}{d\tau} = -2\alpha_1 \omega_G^2 \rho_i^2 \overline{s}^2 \tag{40}$$

which can be solved by separation of variables with the following result:

$$\frac{1}{\overline{s}} - \frac{1}{\overline{s}_0} = 2\alpha_1 \omega_G^2 \rho_i^2 \tau \;\rightarrow\; \overline{s} = \frac{\overline{s}_0(\tau)}{1 + 2\alpha_1 \omega_G^2 \rho_i^2 \overline{s}_0 \tau} \tag{41}$$

Physically, it is clear that the behavior of the wave beam width, or, in other words, the beam convergence or divergence, is coupled with the curvature of the wave front. The complex solution $\overline{s} = s(\tau) + i\phi(\tau)$ describes the radius of curvature of the phase front R and the width of the packet W through:

$$s(\tau) = \frac{\omega/c}{R(\tau)} \qquad \phi(\tau) = \frac{2}{W^2(\tau)} \tag{42}$$

thus, we have from Eq. 41 the following expression:

$$s(\tau) = \frac{2\alpha_1 \omega_G^2 \rho_i^2 \tau}{1 + 4\alpha_1^2 \omega_G^4 \rho_i^4 \phi_0^2 \tau^2} \qquad \phi(\tau) = \frac{\phi_0}{1 + 4\alpha_1^2 \omega_G^4 \rho_i^4 \phi_0^2 \tau^2} \tag{43}$$

The quantities $s(\tau)$ and $\phi(\tau)$ are related to the s and ϕ quantities respectively described in the previous section. The parameter τ is related to the time t through:

$$\frac{dt}{d\tau} = -\frac{\partial H}{\partial \omega} = 2\omega \tag{44}$$

which at the center of the wave packet yields $\tau = t/(2\omega_G)$. We assume no initial "focusing" so that the initial condition is $s_0 = 0$ and $\phi_0 = 2/W_0^2$. Then, the solution for the evolving width of the packet is:

$$s(t) = \frac{\alpha_1 \omega_G \rho_i^2 \phi_0^2 t}{1 + \omega_G^2 \alpha_1^2 \rho_i^4 \phi_0^2 t^2} \qquad \phi(t) = \frac{\phi_0}{1 + \omega_G^2 \alpha_1^2 \rho_i^4 \phi_0^2 t^2} \tag{45}$$

The explicit expression for the width of the packet is

$$W^2(t) = W_0^2\Big[1 + \Big(\frac{2\omega_G \alpha_1 \rho_i^2 t}{W_0^2}\Big)^2\Big] \tag{46}$$

We observe that Eq. 23 and Eq. 46 are the same and we can associate a GAM refraction-index n_G to the equilibrium conditions for the GAM evolution. Practically, we know which are the principal properties and characteristics of the equilibrium that influence the behavior of GAMs. We note that the curvature $s(t)$ of the wave front depends on the sign of α_1. In Fig. 2 we show an example of the solution obtained as:

$$u(r,t) = \exp\{\frac{1}{2}[is(t)(r-0.5)^2 + \phi(t)(r-0.5)^2] - i\omega_G t\} \tag{47}$$

We observe a convex (top panel) and a concave (bottom panel) wave front of the beam for a negative and a positive value respectively of the α_1 parameter. For an α_1 value equal to zero the wave front assumes a straight shape (not shown). It is worth to note that a similar anomalous lens effect has been described in Ref. 51 for a beam that propagates in homogeneous magnetoplasmas. We emphasize that in our case the GAM beam propagates in a space-time plane.

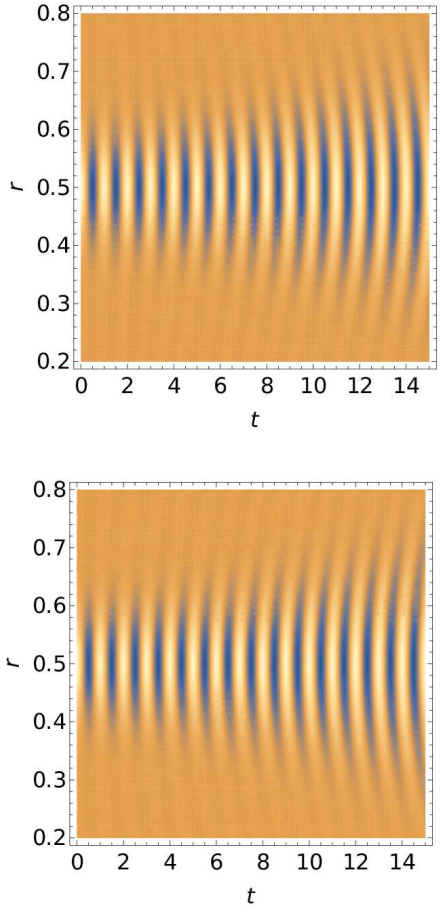

FIG. 2. *Example of time evolution of GAM electric field from Eq. 47 with initial Gaussian profile oscillating in a homogeneous equilibrium for a negative (top panel) and a positive (bottom panel) value of* α_1.

B. Inhomogeneous case

The paraxial WKB method can be easily extended to the inhomogeneous one-dimensional case. To this purpose we consider a temperature gradient $1/L_T$ different from zero. The relevant Hamiltonian is still given by Eq. 35

$$H = \omega_G^2\Big(1 - \frac{r-r_0}{L_T}\Big)(1+\alpha_1 k_r^2\rho_i^2) - \omega^2 \qquad (48)$$

The trajectory of the center of the Gaussian packet is identical to the ray corresponding to $p = 0$ in the treatment presented in Sec. III. From Eq. 37 and Eq. 38, the following derivatives are needed in order to solve explicitly the paraxial equations:

$$\frac{\partial^2 H}{\partial r^2} = 0 \qquad \frac{\partial^2 H}{\partial k_r^2} = 2\alpha_1\omega_G^2\rho_i^2\Big(1 - \frac{r-r_0}{L_T}\Big) \qquad (49)$$

$$\frac{\partial^2 H}{\partial r \partial k_r} = -2\alpha_1\rho_i^2\frac{\omega_G^2}{L_T}k_r \qquad \frac{\partial H}{\partial r} = \frac{-\omega_G}{L_T}(1+\alpha_1 k_r^2\rho_i^2) \qquad (50)$$

$$\frac{\partial H}{\partial k_r} = 2\alpha_1\omega_G^2\rho_i^2\Big(1 - \frac{r-r_0}{L_T}\Big)k_r \qquad (51)$$

It can be noticed that the assumption of a linear temperature profile, leading to a vanishing second derivative with respect to r, implies that the Riccati equation for $\overline{s}$ takes the form of a Bernoulli differential equation, which can be readily solved for its inverse $u = 1/\overline{s}$. Eq. 38 can be written in this case:

$$\frac{du}{d\tau} - 2\frac{\partial^2 H}{\partial r \partial k_r}u = \frac{\partial^2 H}{\partial k_r^2} \qquad (52)$$

$$u(\tau) = e^{-F(\tau)}\Big(u_0 + \int_0^\tau \frac{\partial^2 H}{\partial k_r^2}(\tau')e^{-F(\tau')}d\tau'\Big) \qquad (53)$$

with

$$F(x) = -2\int_0^x \frac{\partial^2 H}{\partial k_r \partial r}(y)dy \qquad (54)$$

In the homogeneous limit considered in the previous section, $F = 0$ and Eq. 53 reproduces Eq. 41.

V. SIMULATION RESULTS AND COMPARISON WITH OPTICAL THEORY

In order to verify the applicability of the optical methods to the GAM dynamics, we performed several simulations with the gyrokinetic code ORB5. In all the simulations we assume flat density and safety factor profiles. We note that without a drive source, the dissipation effects can be very strong, overtaking the dispersion effects. We recall that Landau damping is the principal reason of GAM dissipation and moreover it can be strongly amplified in the presence of a temperature gradient[20–23]. Here, we will neglect the dissipation effects. In other words, we consider the dispersion relation of GAMs $\omega + i\gamma_L$ with:

$$\gamma_L = -f(v_{T_i}, q, \tau_e) + k_r^2 g(v_{T_i}, q, \tau_e) \qquad (55)$$

where $f(v_{T_i}, q, \tau_e)$ and $g(v_{T_i}, q, \tau_e)$ are functions describing finite Larmor radius and finite orbit width effects respectively[18,19] and we choose a range of values for which both $|f|$ and $|g|$ are very small. In Fig. 3 we show the two $|f|$ and $|g|$ expressions (with $|g|$ normalized to the minor radius) as a function of the safety factor q and of the ratio between electron and ion temperatures τ_e. We observe that increasing the value of τ_e and of the safety factor the dissipation drastically decreases. Consequently, we first consider simulations with a safety factor value $q = 3$ and with $\tau_e > 17$ in order to emphasize the dispersive effects described by the theory. Moreover we assume homogeneous density and safety factor, an inverse aspect ratio $\epsilon = 0.1$, a diameter $L_r = 2/\rho^* = 320$ with $\rho^* = \rho_s/a$. All the simulations utilize the electrostatic version of the gyrokinetic model and consider a hydrogen plasma with adiabatic electrons.

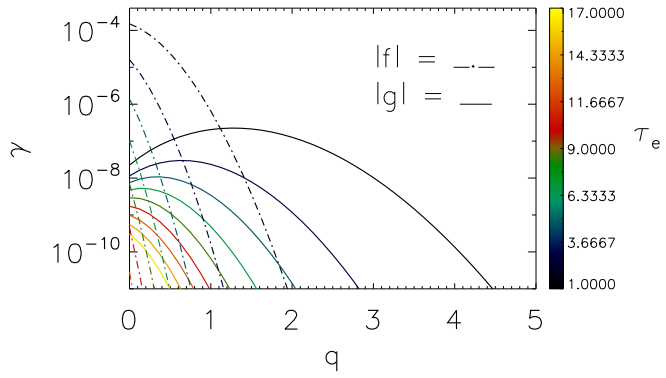

FIG. 3. $|f|$ and $|g|$ functions appearing in the damping rate γ_L. $|f|$ and $|g|$ are shown as a function of q for several values of τ_e.

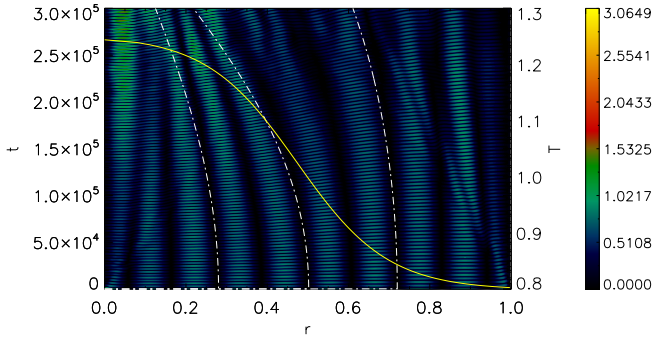

FIG. 4. Absolute value of the GAM electric field as a function of time and radial coordinate. The signal is initialized as $E(r) = \cos(\pi k_r r)$ with $k_r = 10$. Overlapped, the considered temperature profile and the $r(t)$ trajectories of different radial nodes are shown.

First, we consider the time evolution of a single mode for a GAM that evolves in an equilibrium with the following temperature profile:

$$T(r) = \exp\{-\kappa_T l \tanh[(r - r_0)/l]\} \tag{56}$$

with $l = 0.225$, $\kappa_T = 1.0$ and $r_0 = 0.5$ (the temperature profile is taken identical for ions and electrons in order to keep τ_e constant across the radius). Thus we choose a radial signal initialized as $E(r) = \cos(\pi k_r r)$ with a radial $k_r = 10$ value. Because we have no beam signal in this case, the spreading term in Eq. 34 is not relevant. In other words, the problem is reduced to find the dynamics of nodes or peaks of the cosine signal. Therefore, by imposing $p = 0$ in Eq. 34 we obtain the trajectories of nodes that correspond to the ray path:

$$r(t) = \frac{t^2}{2}\Big[+ \frac{1}{2}\alpha_1 \rho_i^2 \omega_G^2 \frac{1}{L_T}\Big] + r_N \tag{57}$$

with r_N initial position of the N-node. We recall that, for large τ_e, the parameter α_1 in the GAM dispersion relation is negative and the corresponding radial propagation is directed inwards. Moreover, we note that Eq. 57 has been validated also in more realistic conditions with $\tau_e \approx 1$ relevant for experiments[23]. For these realistic values of τ_e, Eq. 57 shows that the GAM propagation is also important and directed outwards. In Fig. 4 we find the time evolution of the signal and overlapped the temperature profile and the trajectories $r(t)$. In the calculation of the trajectories the local effect of the temperature value is taken into account. It is interesting to observe that as in a magnifying-glass the rays converge where the concavity of the temperature is positive and diverge where the concavity is negative. Thus, in a driveless system in which the GAM can be only damped we can increase locally the amplitude of the oscillations by focusing the GAM energy. We observe also a small discrepancy between theoretical and numerical trajectories at large time. This could reflect a small difference in the α_1 value related to the analytical and numerical calculation.

In order to study dispersive effects, we choose a Gaussian packet for GAM that, on the basis of the previous considerations, evolves in time as a Gaussian beam that propagates in two space dimensions. For this case we consider a flat temperature profile. The results are shown in Fig. 5 in which we present the time evolution of two GAM Gaussian profiles with two different width values $W_0 = 0.04$ (top panel) and $W_0 = 0.02$ (bottom panel). Hereafter, unless noted otherwise, with respect to the orientation of the axis of Fig. 4 we plot the absolute value of the GAM electric field in the (t, r) plane. Overlapped, we plot the phase path predicted by Eq. 34 (white lines). We observe that the theory well reproduces the spreading of the GAM packet. In particular the spreading increases by decreasing the value of W_0. Moreover, the spreading increases in time in agreement with the value of the refraction index associated to the equilibrium conditions. Thus, the spreading of GAM in time can be predicted and interpreted as a diffraction effect. It is interesting to observe that the beam first spreads with a parabolic shape and after increases in a hyperbolic way. By continuing the parallel with light beam we can associate to the GAM evolution a "Rayleigh time":

$$t_R = \frac{W_0^2}{2|\alpha_1|\omega_G \rho_i^2} \tag{58}$$

We recall that in optics the Rayleigh length is a collimation distance that characterizes the divergent nature of the optical beam. The Rayleigh length (or Rayleigh range) of a laser beam is the distance from the beam waist (in the propagation direction) where the beam radius increases by a factor of the square root of two.

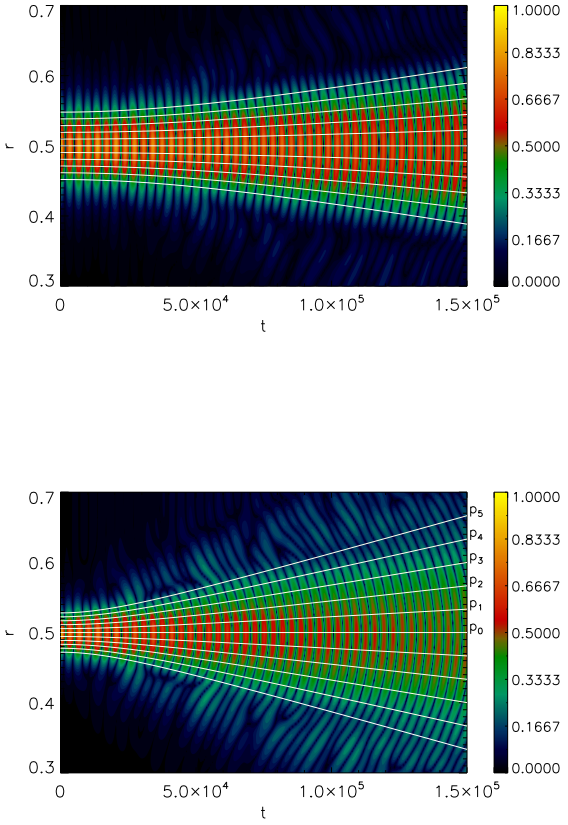

FIG. 5. *Time evolution of the absolute value of the GAM electric field profiles oscillating in a homogeneous equilibrium for two different values of W_0. The overlapped phase-path trajectories (white lines), predicted analytically, well reproduce the spreading of GAMs.*

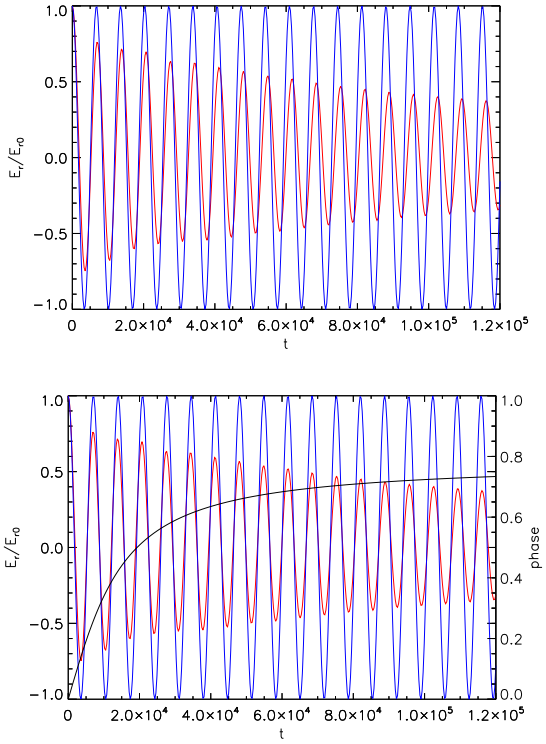

FIG. 6. *(Top panel) Time evolution of GAM electric field for the Gaussian radial profile with $W_0 = 0.02$ (red line) and GAM signal that oscillates with ω_G frequency (blue line). (Bottom panel) Time evolution of GAM electric field for the Gaussian radial profile with $W_0 = 0.02$ (red line) and theoretical GAM signal oscillation (blue line) that includes the absolute value of the Gouy phase shift (black line).*

For the two cases of Fig. 5 with $W_0 = 0.04$ and $W_0 = 0.02$ we find $t_R = 5 \cdot 10^4 \Omega_i^{-1}$ and $t_R = 1.25 \cdot 10^4 \Omega_i^{-1}$ respectively. Moreover, for both simulations we adopt $\tau_e = 40$ with the associated $\alpha_1 = -8.89$. We can continue the correspondence between the time evolution of GAM oscillations and a spatial light beam propagation, by observing that the latter involves a not obvious and important additional *phase shift* named Gouy phase. Thus, in addition to the fixed wave phase in $e^{-i(t\omega_G)}$ there is also a temporal cumulative axially phase shift $\psi(t)$ related to the curvature of the wave front of GAMs in the space-time plane:

$$\psi(t) = \frac{1}{2}\frac{\alpha_1}{|\alpha_1|}\arctan\left(\frac{t}{t_R}\right) \tag{59}$$

The coefficient 1/2 in Eq. 59 is due to the fact that in our problem there is only one transverse direction[52]. In order to put in evidence this phase shift, in the top panel of Fig. 6 we plot the time evolution of the GAM electric field at $r = 0.5$ for the case with $W_0 = 0.02$ (red color) and the time evolution of a GAM signal that oscillates at the frequency ω_G (blue color). The comparison between the two signals emphasizes the effect of the Gouy shift that change in time the GAM phase related to the simulation result. In the bottom panel we compare the same previous GAM signal obtained by simulation and the analytical signal (blue line) predicted by considering the Gouys effect of Eq. 59 in GAM oscillation $e^{-i[t\omega_G+\psi(t)]}$. The Gouy phase $|\psi(t)|$ is also plotted in the same figure (black line). The comparison between the two signal suggests a new method to enhance the accuracy of the value determination of α_1 by simulation results. In fact, the Gouy phase is directly related to the dispersion relation and in particular to the α_1 value via the Rayleigh time t_R. We emphasize that in our case the Gouy phase shift corresponds to a temporal shift on the oscillation frequency. This Gouy effect can be responsible for the slightly different resonance frequencies and mode beats and can play a role during the interaction of GAMs with turbulence. This latter aspect will be object of a future work.

An important test for the applicability of optical theories to GAM dynamics is represented by the energy conservation. In particular the energy must be conserved

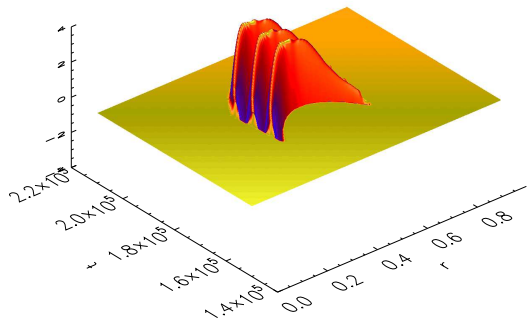

FIG. 7. Three oscillations of GAM in the (r,t)-plane selected by a Mask calculated analytically by considering the phase paths and the wave fronts. The mask can be adapted in order to select the energy evolution contained in a flux tube characterized by two phase paths p_i, p_{i+j}.

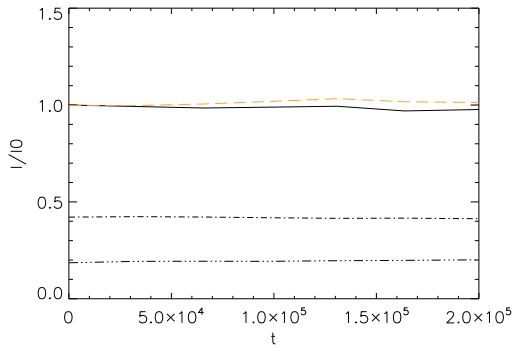

FIG. 8. Time evolution of energy calculated by following in time the average of energy of three GAM oscillations (see Fig. 7 and bottom panel of Fig. 5)

in a flux tube between two generic phase-paths p_1 and p_2. In order to investigate the conservation of energy, we have developed a diagnostic that by means of a mask in the (t,r)-plane can find the GAM wave fronts evolution (see Fig. 7). This mask has been calculated by considering the phase paths given by Eq. 34 and the wave front shape given by Eq. 45. In this way it is even possible to find the transport of the energy inside a specific flux tube. In particular the figure shows three oscillation in time of an initial gaussian packet whose "wave-front" evolves in the (r,t) plane. We apply this diagnostic to the previous case with $W_0 = 0.02$ and $\tau_e = 40$ in which only dispersive effects are retained. For this case we consider the beam contained between the phase-paths characterized by $p_i = 0.035r$ and $p_{-i} = -0.035r$. We recall that p is the parameter that identifies a phase-path by mean of the distance from the center of the packet. Thus, we consider the 98% of the surface of the beam and we find in time the associated energy related to the wave front of three oscillations of the beam. In Fig. 8 we plot the time evolution of this energy normalized to the initial energy I_0 of three oscillations and we observe that it is conserved with a good approximation (black continuous line).

We consider also the time evolution of the energy always related to three waves but contained between the flux tube inner p_4 and p_0 phase path (three dotted dash line) and between p_1 and p_0 (see bottom panel of Fig. 5) with $p_0 = 0$ center of the packet. In this way we estimate that the energy contained inside the flux tube $p_4 - p_0$ is two time the energy inside $p_1 - p_0$ and in both of cases the energy is conserved (dash dotted line). We make emphasis again on the fact that our wave front develops in a space-time plane. Because we live in a universe in which we can observe single spatial surfaces (foliations), it is important to verify the energy conservation also between two temporal steps. Therefore, we consider the temporal interval between three oscillations with $\Delta t_o = 3{\cdot}2\pi\omega_G^{-1} = 20700\Omega_i^{-1}$. The energy integrated in the radial range $0 \leqslant r \leqslant 1$ and between two temporal steps $t_i - (t_i + \Delta t_o)$ is conserved (orange dashed line). We note that the energy quantity between a time range Δt_o is more or less the same that one of the wave front of three waves that evolve in the (r,t)-plane. The accuracy of the calculation of energy conservation depends principally on the code for the orange line and depends both on the code and on the precision of the analytical phase-path trajectories for the black continuous line. This justifies the small difference between the two lines and at the same time shows the reliability of the optical methods.

Due to the fact that we adopt an optical beam analysis we expect a spreading behavior similar to that of a Gaussian beam also for different beam shapes. In fact Gaussian beam is only the lowest-order solution in an infinite family of higher-order beam-like solution of the Helmholtz equation. Very interesting are solutions with non-Gaussian distributions but that share the paraboloidal wave fronts of the Gaussian beam. These functions are known as the Hermite-Gaussian function whose zero-order corresponds to the Gaussian shape. Thus, we investigate the behavior of functions different from the Gaussian packet and we consider a GAM signal initialized with a first-order Hermite-Gaussian beam $E \sim x\exp(-x^2/W_0^2)$ with $W_0 = 0.02$. This signal oscillates in an equilibrium with flat temperature profile. In agreement with the theory we obtain a spreading similar to the corresponding Gaussian case. The time evolution of this signal is shown in Fig. 9.

As a further verification of the optical theory applied to GAM structures we consider the time evolution for the Gaussian beam in an equilibrium with flat temperature profile and in which we switch-off the dispersive effects. To this purpose we recall that dispersive effects are related to the α_1 value. This parameter assumes values around zero for $\tau_e = 6$ (see Ref.s 17, 23, and 50). By

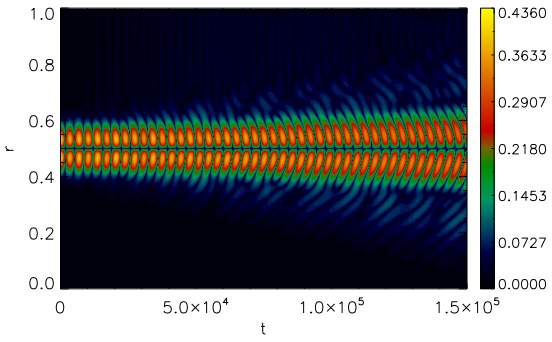

FIG. 9. Absolute value of the GAM electric field as a function of time and radial coordinate. The signal is initialized with a first-order Hermite-Gaussian function in the (t, r) plane.

assuming this τ_e value, in Fig. 10 we show the evolution of two packet with $W_0 = 0.04$ and $W_0 = 0.02$ respectively. The wave fronts are straight lines in agreement with the expected results by considering $\alpha_1 \approx 0$ in the GAM dispersion relation and in Eq. 45. We observe an eigenmode oscillation for the considered GAM signal. Despite the fact that the same structure evolution is observed for both cases of Fig. 10, the GAM amplitude in the bottom panel decreases faster than that one of the GAM in the top panel. Because dispersion effects are zero, this behavior of GAMs is due to the dissipation. For $\tau_e = 6$ the dissipation effects are important and energy is efficiently dissipated with the increase of k_r values (see Eq. 55). The Fourier transform of the signal with $W_0 = 0.02$ shows that the energy is distributed on a larger spectrum than one of the signal with $W_0 = 0.04$. Consequently, in the presence of a strong dissipation for higher k_r mode the narrow packet is damped faster than the broad packet. A detailed analysis of the dissipative behavior of GAMs is in preparation.

As last case we would like to verify the validity of Eq. 34 by considering dispersion effects in the presence of a temperature gradient. Thus, we perform a simulation in which a GAM, initialized with a first-order Hermite-Gaussian signal with $W_0 = 0.02$, propagates in a medium with the temperature profile of Eq. 56 characterized by $l = 0.09$, $\kappa_T = -10.0$ and $r_0 = 0.5$. Moreover, we consider a value $\tau_e = 40$ and we choose a beam with a first-order Hermite-Gaussian function in order to better find the time evolution of the node of the packet that is simpler to identify with respect to the peak of the Gaussian signal. In this way, we recall that we find the time evolution of the ray tracing trajectory. The results are shown in Fig. 11 in which we have the electric field evolution of the GAM beam and overlapped the phase path predicted by the theory for the ray tracing and for the

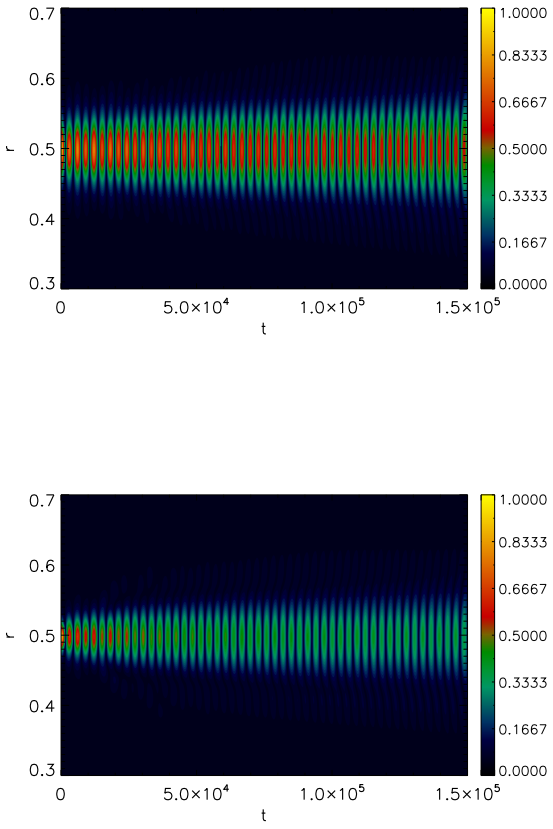

FIG. 10. Absolute value of the GAM electric field as a function of time and radial coordinate. The signals in top and bottom panels present two different width W_0 respectively. In order to quench the dispersive effects ($\alpha_1 = 0$ condition) we have considered $\tau_e = 6$.

spreading of GAM. In this simulation we can appreciate the power and efficiency of the geometrical optical methods in the description of radial-temporal evolution of GAM packet. We emphasize the parallel between the trajectory in the space time of a GAM signal that evolves in the presence of a nonuniform tokamak equilibrium and the trajectory of a light beam that propagates in a space plane in a medium with an inhomogeneous index of refraction. In light of the obtained results by observing Fig. 11 we can give an elegant and new interpretation of the Phase-mixing. In fact, this phenomenon appears as the projection along the radial plane at a fixed time of the wave front that evolves in a space-time plane. At the same time, the evolution of GAM frequency can be see as the projection at a fixed radial position of the wave front along the temporal direction. We observe that the effects of diffraction related to the value of equilibrium parameters and the effects of propagation related to the parameter gradients are enclosed in the radial evolution

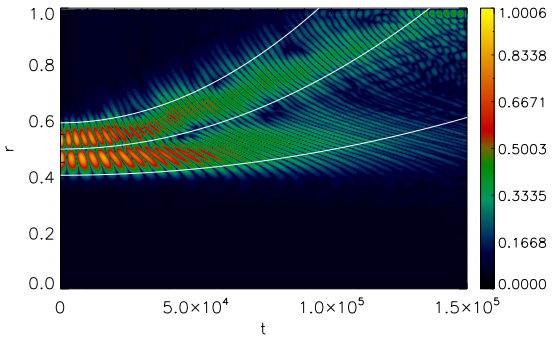

FIG. 11. Absolute value of the GAM electric field as a function of time and radial coordinate. The signal, initialized with a first-order Hermite-Gaussian function, evolves in the presence of a temperature gradient in the (t, r) plane. Overlapped we plot the central and the boundary trajectories of the beam.

of the GAM signal.

VI. CONCLUSIONS

The dynamics of GAMs has been investigated by means of optical methods. In particular we used complex eikonal techniques to investigate in an original way the time evolution of a GAM represented by means of an Hermite-Gaussian packet. The applicability of methods and their efficacy have been tested by means of a comparison with gyrokinetic simulations that has confirmed all the aspects predicted by the theory. In particular we showed how it is possible to associate a GAM refraction-index n_G for the GAM structures to the equilibrium conditions. In other words we have indicated by means of a n_G quantity the combination of parameters that influences the radial propagation and shape evolution of GAMs in the tokamak devices. In this work we have continued previous investigations[23] arriving to obtain a more and more detailed description of the GAM dynamics. In this way we have reached a high understanding level through which the nonlinear effects linked to the turbulence-drive are more and more isolated. We can predict with an elevate precision the propagation of the energy related to the GAMs simplifying in this way the interpretation of GAM/turbulence interaction in nonlinear simulations and in the experiments. We have demonstrated the applicability of optical techniques to the GAM dynamics prediction also for complicated profiles of these structures that can be, thus, described by means of high-order Hermite-Gaussian functions.

We observe that from the mathematical point of view, solving the quasi-optical equations in the presence of a source can be addressed employing a Wigner function formalism, which will be subject of a subsequent paper. The physical picture given in the paper for the dynamics of a spreading packet should remain valid also in this case. Moreover, this paper introduces new instruments to describe GAM evolution, such as Rayleigh time and Gouy phase, wave-front and phase-path in space-time plane. These instruments allowed us to give a very elegant interpretation of the Phase-mixing and frequency evolution of GAM oscillations. In particular, these methods establish a correlation between the time evolution of the shape and of the frequency of GAMs helping in this way to understand and to predict the interaction of these structures with modes and turbulence perturbations. We emphasize that a similar geometrical description of GAM properties can be applied to other structures in tokamak devices such as drift waves and so on. Thus, we find a very efficient and intuitive manner to describe multifaceted phenomena. In fact in this way different structures can interact between them, via specific like-index of refraction associated to the environment in which these structures evolve.

ACKNOWLEDGMENTS

Interesting and useful discussions with G. D. Conway, A. Ghizzo and O. Maj and support by Eurofusion Enabling Research projects ENR-MFE19.MPG-01 and "NAT" (WP17-ER/MPG-01) are kindly acknowledged. This work has been carried out within the framework of the EUROfusion Consortium and has received funding from the Euratom research and training programme 2014-2018 and 2019-2020 under grant agreement No 633053. The views and opinions expressed herein do not necessarily reflect those of the European Commission.

[1] B. N. Rogers, W. Dorland, and M. Kotschenreuther, *Phys. Rev. Lett.* **85**, 5336 (2000).
[2] Eun-jin Kim and P. H. Diamond, *Phys. Plasmas* **9**, 4530 (2001).
[3] A. Fujisawa, K. Itoh, H. Iguchi, K. Matsuoka, S. Okamura, A. Shimizu, T. Minami, Y. Yoshimura, K. Nagaoka, C. Takahashi, M. Kojima, H. Nakano, S. Ohsima, S. Nishimura, M. Isobe, C. Suzuki, T. Akiyama, K. Ida, K. Toi, S.-I. Itoh, and P. H. Diamond, *Phys. Rev. Lett.* **93**, 165002 (2004).
[4] P.H. Diamond, S.-I. Itoh, K. Itoh, and T. S. Hahm, *Plasma Phys. Controlled Fusion* **47**, 35 (2005).
[5] C. Holland and P. H. Diamond, *Phys. Lett. A* **344**, 369 (2005).
[6] F. Palermo, X. Garbert, and A. Ghizzo, T. Cartier-Michaud, P. Ghendrih, V. Grandgirard, and Y. Sarazin, *Phys. Plasmas* **22**, 042304 (2015).
[7] F. Palermo, X. Garbet, A. Ghizzo, *Europ. Phys. Journal D* **69**, 8 (2015).
[8] A. Ghizzo and F. Palermo, *Phys. Plasmas* **22**, 082303 (2015).
[9] A. Ghizzo and F. Palermo, *Phys. Plasmas* **22**, 082304 (2015).
[10] N. Winsor, J. L. Johnson, and J. M. Dawson, *Phys. Fluids* **11**, 2448 (1968).
[11] B. Scott, *Phys. Lett. A* **320**, 53 (2003).
[12] S Satake, M Okamoto, N Nakajima, H Sugama, M Yokoyama, C.D Beidler *Nucl. Fusion* **45**, 1362 (2005)
[13] S. Satake, H. Sugama and T.-H. Watanabe *Nucl. Fusion* **47**, 1258 (2007).
[14] G.D. Conway, C. Tröster, B. Scott, K. Hallatschek and the AS-

DEX Upgrade Team, *Plasma Phys. Control. Fusion* **50**, 055009 (2008).
[15]C. A. de Meijere, S. Coda, Z. Huang, L. Vermare, T. Vernay, V. Vuille, S. Brunner, J. Dominski, P. Hennequin, A. Krmer-Flecken, G. Merlo, L. Porte and L. Villard, *Plasma Phys. Control. Fusion* **56**, 072001 (2014).
[16]G. D. Conway, B. Scott, J. Schirmer, M. Reich, A. Kendl and the ASDEX Upgrade Team, *Plasma Phys. Control. Fusion* **47**, 1165 (2005).
[17]F. Zonca and L. Chen, *Europhys. Letter* **83**, 35001 (2008).
[18]H. Sugama and T.-H. Watanabe *J. Plasma Phys.* **72**, 825 (2006).
[19]H. Sugama and T.-H. Watanabe *J. Plasma Phys.* **74**, 139 (2008).
[20]F. Palermo, A. Biancalani, C. Angioni, F. Zonca, A. Bottino, *Europhys. Letter* **115**, 15001 (2016).
[21]F. Palermo, A. Biancalani, C. Angioni, F. Zonca, A. Bottino, G. Conway and E. Poli, 43^{rd} *EPS Conf. Plasma Physics*, P1.046 (2016).
[22]A. Biancalani, F. Palermo, C. Angioni, A. Bottino, F. Zonca, *Phys. Plasmas* **23**, 112115 (2016).
[23]F. Palermo, E. Poli, A. Bottino, A. Biancalani, G. D. Conway and B. Scott *Physics of Plasma* **24**, 072503 (2017).
[24]K. Itoh, S-I. Itoh, P. H. Diamond, A. Fujisawa, M. Yagi, T. Watari, Y. Nagashima and A. Fukuyama, *Plasma and Fusion Research: Rapid Communications* **1**, 037 (2006).
[25]J. C. Hillesheim, W. A. Peebles, T. A. Carter, L. Schmitz, and T. L. Rhodes *Phys. Plasmas* **19**, 022301 (2012).
[26]P. Simon, Investigation of geodesic acoustic mode flow oscillations using Doppler reflectometry in ASDEX Upgrade PhD Thesis University de Lorraine, PhD Thesis, *Univ. Stuttgart* (2017).
[27]T. Ido, Y. Miura, K. Hoshino, K. Kamiya, Y. Hamada, A. Nishizawa, Y. Kawasumi, H. Ogawa, Y. Nagashima, K. Shinohara, Y. Kusama, JFT-2M group, *Nucl. Fusion* **46**, 512 (2006).
[28]Y. Xu, I. Shesterikov, M. Van Schoor, M. Vergote, R. R. Weynants, A. Krmer-Flecken, S. Zoletnik, S. Soldatov, D. Reiser, K. Hallatschek, C. Hidalgo, *Plasma Phys. Control. Fusion* **53** 095015 (2011).
[29]A. D. Gurchenko, E. Z. Gusakov, P. Niskala, A. B. Altukhov, L. A. Esipov, T. P. Kiviniemi, T. Korpilo, D. V. Kouprienko, S. I. Lashkul, S. Leerink, A. A. Perevalov and M. A. Irzak, *Plasma Phys. Control. Fusion* **58**, 044002 (2016).
[30]D. F. Kong, A. D. Liu, T. Lan, Z. Y. Qiu, H. L. Zhao, H. G. Sheng, C. X. Yu, L. Chen, G. S. Xu, W. Zhang, B. N. Wan, R. Chen, W. X. Ding, X. Sun, J. L. Xie, H. Li and W. D. Liu *Nucl. Fusion* **53**, 113008 (2013).
[31]M. Sasaki, K. Itoh, T. Kobayashi, N. Kasuya, A. Fujisawa, S. I. Itoh, *Nucl. Fusion* **58**, 112005 (2018).
[32]R. Hager and K. Hallatschek, *Phys. Plasmas* **16**, 072503 (2009).
[33]Z. Qiu, F. Zonca and L. Chen, *Plasma Science and Technology* **13**, 257 (2011).
[34]E. Mazzuccato, *Phys. Plasmas* **1**, 1855, (1989).
[35]S. Choudhary and L. B. Felsen, *IEEE Trans. Antennas Propag.* **21**, 827, (1973).
[36]S. Choudhary and L. B. Felsen, *IEEE Trans. Antennas Propag.* **62**, 1530, (1974).
[37]G. V. Pereverzev, *Physics of Plasmas* **8**, 3664 (2001).
[38]G. V. Pereverzev, *Reviews of Plasma Physics*, 19 Consultants Bureau, New York-London (1996)
[39]G. V. Pereverzev, *Phys Plasmas* 5, 3529 (1998).
[40]E. Poli, G. V. Pereverzev and A. G. Peeters, *Phys. Plasmas* 6, 5, (1999).
[41]S. Jolliet, A. Bottino, P. Angelino, R. Hatzky, T. M. Tran, B. F. McMillan, O. Sauter, K. Appert, Y. Idomura, and L. Villard, *Comput. Phys. Commun.* **177**, 409 (2007).
[42]A. Bottino, T. Vernay, B. Scott, S. Brunner, R. Hatzky, S. Jolliet, B. F. McMillan, T. M. Tran and L. Villard, *Plasma Phys. Controlled Fusion* **53**, 124027 (2011).
[43]A. Bottino and E. Sonnendrücker, *J. Plasma Phys.* **81**, 435810501 (2015).
[44]E. Lanti, N. Ohana, N. Tronko, T. Hayward-Schneider, A. Bottino, B. F. McMillan, A. Mishchenko, A. Scheinberg, A. Biancalani, P. Angelino, S. Brunner, J. Dominski, P. Donnel, C. Gheller, R. Hatzky, A. Jocksch, S. Jolliet, Z.X. Lu, J. P. Martin Collar, I. Novikau, E. Sonnendrcker, T. Vernay and L. Villard *Submitted to Computer Physics Communications*
[45]N. Tronko, Bottino A. and E. Sonnendrücker, *Phys. of Plasmas*, **23**, 082505 (2016).
[46]T.S. Hahm, W.W. Lee and A. Brizard, *Phys. Fluids* **31**, 1940 (1988).
[47]A.J. Brizard and T.S. Hahm, *Rev. of Modern Phys.* **79**, 421 (2007).
[48]H. Sugama, *Phys. Plasmas* **7**, 466 (2000).
[49]B. Scott and J. Smirnov, *Phys. Plasmas* **17**, 112302 (2010).
[50]A. I. Smolyakov, M. F. Bashir, A. G. Elfimov, M. Yagi, and N. Miyato, *Plasma Physics Reports* **42**, 407 (2016).
[51]R. Sugihara and H. Shamoto *Physics Letters A* **280**, 340 (2001).
[52]M. Bornatici and O. Maj, *Plasma Phys. Control. Fusion* **45**, 707 (2003).